# Polymer-mediated adhesion: nanoscale surface morphology and failure mechanisms

Alberto Baggioli, Mosé Casalegno, Alessio David, Marta Pasquini, and Guido Raos*

*Department of Chemistry, Materials and Chemical Engineering "G. Natta", Politecnico di Milano, Via L. Mancinelli 7, I-20131 Milano, Italy*

E-mail: guido.raos@polimi.it

**Abstract**

We present coarse-grained molecular dynamics simulations of polymer-mediated adhesion between chemically heterogeneous surfaces. Our surface models exhibit weakly and strongly absorbing sites in 1:1 proportion, but are characterized by different degrees of segregation among these sites. When the surfaces are pulled apart, we observe systematic variations in the stress-strain curves, indicating a significant weakening of the adhesive layer on going from finely interdispersed to more segregated morphologies. In our model systems, the macroscopic failure of the sandwiched polymer films always appears to be cohesive but, at the nanoscale, there is in fact a gradual transition from a cohesive to a mixed cohesive-adhesive mechanism.

**Introduction.** Adhesion phenomena involving polymers and other soft materials are relevant for many technologies, and they provide a wealth of fascinating observations and challenging problems.[1] Many aspect of polymer-mediated adhesion can be described by continuum-based models,[2] but even in these cases the parameters entering them derive from

molecular-level interactions and processes.[3,4] Standardized tests have been developed in order to measure the properties of polymer adhesives at macroscopic length scales,[1] while the surface force apparatus and atomic force microscopy have allowed direct and detailed measurements of analogous phenomena in extremely thin films and at much smaller length scales.[5–7] Much current research is driven by the desire to understand and mimic the adhesive properties of living systems, which range from strong but highly reversible (e.g., in geckos' feet) to extremely tough, even underwater (e.g., in mussels' byssus).[8–11]

When the adhesive is a rubbery polymer, as is the case in pressure-sensitive adhesives (PSAs), large deformations and viscoelasticity become relevant.[12,13] The combination of surface chemistry and roughness, polymer microstructure and morphology, film thickness, temperature and deformation speed produces a wide range of scenarios.[14] In a typical "tack test", two surfaces (adherends) are first brought together and equilibrated, with a polymer adhesive in between. They are then separated at constant speed and the stress is measured until complete detachment. There are two basic outcomes for such an experiment. In the case of *adhesive failure*, which is the intended outcome in PSA applications, the polymer separates neatly from one surface. Stresses are relatively low in this case, but the practical work of adhesion—the integral of the stress-strain curve—is still much larger than any estimate based on intermolecular forces and equilibrium thermodynamics. This demonstrates the importance of energy dissipation and non-equilibrium phenomena. Alternatively, there is the possibility of *cohesive failure*, whereby the polymer film breaks up somewhere in the middle and ends up on both surfaces. This is desirable when the adherends should not separate so easily, and it occurs only when the polymer-substrate interfaces can sustain large stresses. In both cases, breakup involves the initial nucleation of voids or "bubbles" (at the interface or within the polymer, respectively in the adhesive and cohesive scenarios), which then evolve to produce long polymer fibrils bridging the surfaces.[15] Three-dimensional stereoscopic imaging of the cavities have allowed the measurement of finer features, such as the dependence of the receding contact angle on the elastic modulus of the adhesive polymer.[16,17] Subject to

certain conditions and approximations, these observations can be formalized as analytical or numerical models.[18–21] A number of coarse-grained molecular dynamics (MD) simulations have also reproduced different features of polymer-mediated adhesion and film breakup.[22–26]

Phenomena involving highly confined polymers are relevant also for nanocomposites,[27,28] and in particular for rubber reinforcement by carbon black and silica nanoparticles.[29–31] Under large deformations, the rubbery polymer between neighboring particles behaves much like an adhesive layer. In particular, there is several grades of carbon blacks, differing by particle size, morphology and surface chemistry.[32] The best performing fillers expose many asperities and functional groups that interact differently with the polymer chains.[33–35] This produces a geometrically and energetically rough landscape that enhances the mechanical coupling between the polymer and the filler.[36] Cavitation phenomena analogous to those described above for PSAs have also been observed in nanoparticle-filled elastomers undergoing deformation.[37,38] At a more fundamental level, there is also a long-standing interest in understanding of the behavior of polymers in disordered media[39,40] and in thin films, especially close to the glass transition.[41–44]

Previous work by our group addressed different aspects of the previous problems, mostly through *equilibrium* MD simulations of polymers interacting with surfaces incorporating an element of randomness.[45–48] Here we make a step forward, by simulating the *non-equilibrium* adhesive properties of a polymer confined by heterogeneous surfaces. The presence of nanoscale heterogeneities immediately raises some intriguing questions. Does it matter whether the surfaces are chemically heterogeneous, or is the average polymer-surface interaction the only relevant variable? How do the adhesive properties of a polymer film depend on the morphology of the adherend surfaces? Is the distinction between adhesive and cohesive failure of the films still relevant down to the nanoscale, or do we observe other breakup mechanisms?

**Systems and methods.** We have modelled a series of sandwiched polymer systems, similar to those analyzed by Pastore et al.[48]. The surfaces are perfectly rigid, and they

consist of a 50%-50% mixture of weakly ($W$) and strongly ($S$) interacting beads, arranged in a square planar fashion with different morphologies. Each surface consists of $50 \times 50 = 2500$ beads. Starting from either a purely random or a perfectly ordered configuration of the beads, surfaces with different degrees of patchiness have been generated by Monte Carlo simulation of an Ising model with "ferromagnetic" nearest-neighbor interactions.[49] Our Monte Carlo moves involve pairwise exchanges of the identities of $W$ and $S$ sites, and they are accepted or rejected with a Metropolis criterion.[50] Depending on the simulation temperature, the final morphology of the beads may be either dispersed or aggregated. We characterize the final morphology of the surfaces by the Warren-Cowley short-range order parameter $\alpha$.[51,52] This counts the average excess of same-type over opposite-type beads, among the nearest-neighbors of each beads. In order of increasing degree of interdispersion of the $W$ and $S$ sites, the surfaces employed in the following MD simulations have $\alpha \simeq$ 1.0 ($W$ and $S$ beads completely segregated within two parallel stripes), 0.79, 0.53, 0.35, 0.0 (completely random surface), and -1.0 (ordered "checkerboard" configuration). The Supporting Information contains a picture of each surface model (Figure SI.1).

The polymer is modelled using a variant of the Kremer-Grest bead-and-spring model.[53] The maximum FENE (for finitely extensible non-linear elastic) bond length has been slightly reduced in order to limit the surface-induced ordering of the polymer.[54] Note that the bonds of an entangled polymer liquid are susceptible to break at high deformation rates,[55] but for simplicity we have neglected this effect in these simulations.[23] The space between the surfaces is filled with 250 chains of $N = 128$ beads, which is somewhat above the entanglement length for these polymer models. All non-bonded interactions depend on the interparticle distance $r$ and are described by truncated and shifted Lennard-Jones (LJ) potentials:

$$V_{LJ}(r) = 4\varepsilon_{ij}\left[\left(\frac{\sigma}{r}\right)^{12} - \left(\frac{\sigma}{r}\right)^{6}\right] + V_c \qquad r < r_c, \tag{1}$$

where $V_c$ is chosen so that the potential goes continuously to zero at and beyond the cutoff

$r_c = 2.5\sigma$. All beads, belonging either to the polymer or to the confining surfaces, have the same diameter $\sigma$ and the same mass $m$. Instead, the beads differ in their interaction energies. These depend on the type of beads involved ($W$, $S$ or $P$). Relative to polymer-polymer interactions, we have $\varepsilon_{PW} = 0.5\varepsilon_{PP}$ and $\varepsilon_{PS} = 2.0\varepsilon_{PP}$. All simulations were carried out at a temperature $T = \varepsilon_{PP}/k_B$. At this temperature, the bulk polymer behaves as rubbery liquid.

Throughout this manuscript, we adopt the LJ system of reduced units. All quantities are expressed in terms of $\sigma$, $m$ and $\epsilon_{PP}$, and they effectively become adimensional. In particular, pressure and stress are measured in $\epsilon_{PP}/\sigma^3$ units. Time is measured in units of $\tau_{LJ} = \sqrt{m\sigma^2/\epsilon_{PP}}$. The Supporting Information contains a tentative mapping of these quantities to conventional SI units, in order to allow an order-of-magnitude comparison with experimental data on real systems or simulations of detailed atomistic models.

The nearest neighbor distance between the surface beads is equal to 1.0, so that these have an area $A = 2500$. Periodic boundary conditions are enforced in the $x$ and $y$ directions, parallel to the surfaces. The number density of the polymer beads in the middle of the slab is $\rho \simeq 1.05$, equal to the value obtained from constant-pressure simulations of the bulk polymer (at $P = 0.0$). The dynamics of the polymer is simulated by Nose-Hoover style non-Hamiltonian equations of motion[56] with a timestep 0.01 and a relaxation time of 1.00 (both in $\tau_{LJ}$ units). All MD simulations have been carried out with LAMMPS,[57] and the results visualized with VMD.[58]

Table 1: Summary of the main simulation parameters. The parameters that have been varied systematically are highlighted in boldface.

| Description | Value(s) |
|---|---|
| Surface composition | 50% $W$-type and 50% $S$-type beads |
| **Surface morphology** | $\alpha = 1.0$, 0.79, 0.53, 0.35, 0.00 or -1.00 |
| Polymer chain length | $N = 128$ $P$-type beads |
| **Deformation velocity/rate** | $v = 0.10$ ($\dot{\epsilon} = 7.7 \times 10^{-3}$) or $v = 0.01$ ($\dot{\epsilon} = 7.7 \times 10^{-4}$) |
| Interaction energies | $\varepsilon_{PP} = 1.0$, $\varepsilon_{PS} = 2.0$, $\varepsilon_{PW} = 0.5$ |
| Initial inter-surface distance | $z_0 = 13.0$ |
| System size | 250 polymer chains and two $50 \times 50$ surfaces |

For clarity and ease of reference, the main simulation parameters have been collected in Table 1.

**Results.**

In the initial equilibrium configuration, the surfaces are at $z = 0.0$ and $z = 13.0$. The unperturbed root-mean-square radius of gyration of the polymer chains is $R_g = 5.31$. This value, obtained from an independent simulation of the bulk polymer, is comparable with half of the initial inter-surface distance (henceforth $z_0$). As a result, there is an appreciable population of chains forming "bridges", having beads absorbed on both the upper and the lower surface. This is illustrated in Figure SI.2, showing just one of the polymer chains in the initial, undeformed state.

The surfaces, which are assumed to be perfectly rigid, are separated until complete detachment by lifting the upper surface with a constant velocity $v$, which may be either "slow" ($v = 0.01$, in LJ units) or "fast" ($v = 0.1$). These velocities correspond to engineering strain rates $\dot{\epsilon} = v/z_0 = 7.7 \times 10^{-4}$ and $7.7 \times 10^{-3}$, respectively. This allows us to obtain the stress-strain curves for each system. Note that the strain is defined as the ratio between the displacement of the upper surface and the initial inter-surface distance, i.e. $\epsilon(t) = vt/z_0 = \dot{\epsilon}t$. The stress is computed using the virial formula, from the velocities, positions and forces on the polymer beads:[59]

$$\sigma_{zz}(t) = -\frac{1}{V(t)} \sum_{i \in P} \left[ m v_{iz}^2(t) + r_{iz}(t) f_{iz}(t) \right] \tag{2}$$

(note that this is just one element of the full stress tensor, corresponding to the component of the force orthogonal to the surfaces). In this equation $t$ is the time variable and $V(t)$ is the volume occupied by the polymer, which we take equal to $[z_0 + vt - 1] \times A$ (the "-1" approximately corrects for the fact that there is a thin layer next to each surface which is effectively forbidden from being occupied by the polymer, due to the repulsive part of the LJ interactions). The sign in the equation corresponds to the convention adopted when

reporting tack tests on PSA's, i.e. it is positive when the surfaces resist being separated.[12,14] We have also measured the stress from its "macroscopic" definition, namely as the ratio between the pulling force on the upper surface (opposite of sum of the $z$-components of the forces on its beads) and its area $A$. The two definitions lead to results that are comparable, but not identical due to the stochastic nature of the contributions coming from the individual atoms. The larger the system size, the smaller the relative importance of these fluctuations, as they can be expected to decrease as the inverse square root of the number of particles.[60] Therefore the latter are typically noisier, being derived from an average over a smaller number of atoms. We point out that the noise in simulation data has been reduced also by performing a "rolling average", taking care that the averaging window remains much smaller the characteristic time of the investigated phenomena. See Figure SI.5 for plots illustrating this point. One additional advantage of Eq. (2) is that it can be analyzed in terms of individual or local components of the stress, by restricting the summation over a subset of the polymer beads (e.g., those belonging to a specific polymer chain).

Figures 1 and 2 show our numerical results in the initial stages of the deformation, respectively for slow and fast pulling velocities (analogous plots for the full simulations, until complete breakup of the films, are given Figures SI.3 and SI.4). In addition to the stress-strain curves, we also provide plots of the non-bonding component of the potential energy. Although only loosely related, these quantities display a similar behavior as a function of strain. They reveal clear and systematic differences between surfaces with different morphologies. The curves for the random and the ordered checkerboard surfaces ($\alpha = 0$ and $-1$) are very similar, demonstrating that they provide the best adhesion to the polymer. The maxima in the stress at $\epsilon \simeq 0.10$ (slow deformation) and $\epsilon \simeq 0.12$ (fast deformation) correspond to fairly well-defined yield point for these systems. In addition to occurring at higher strains, the yield stress is also larger for the faster deformation, as expected from the viscoelastic nature of the polymer.[20] A faster deformation allows a smaller degree of stress relaxation. Note also that the maxima in the non-bonding energy occur slightly after those

of the stress, especially in the case of fast deformation.

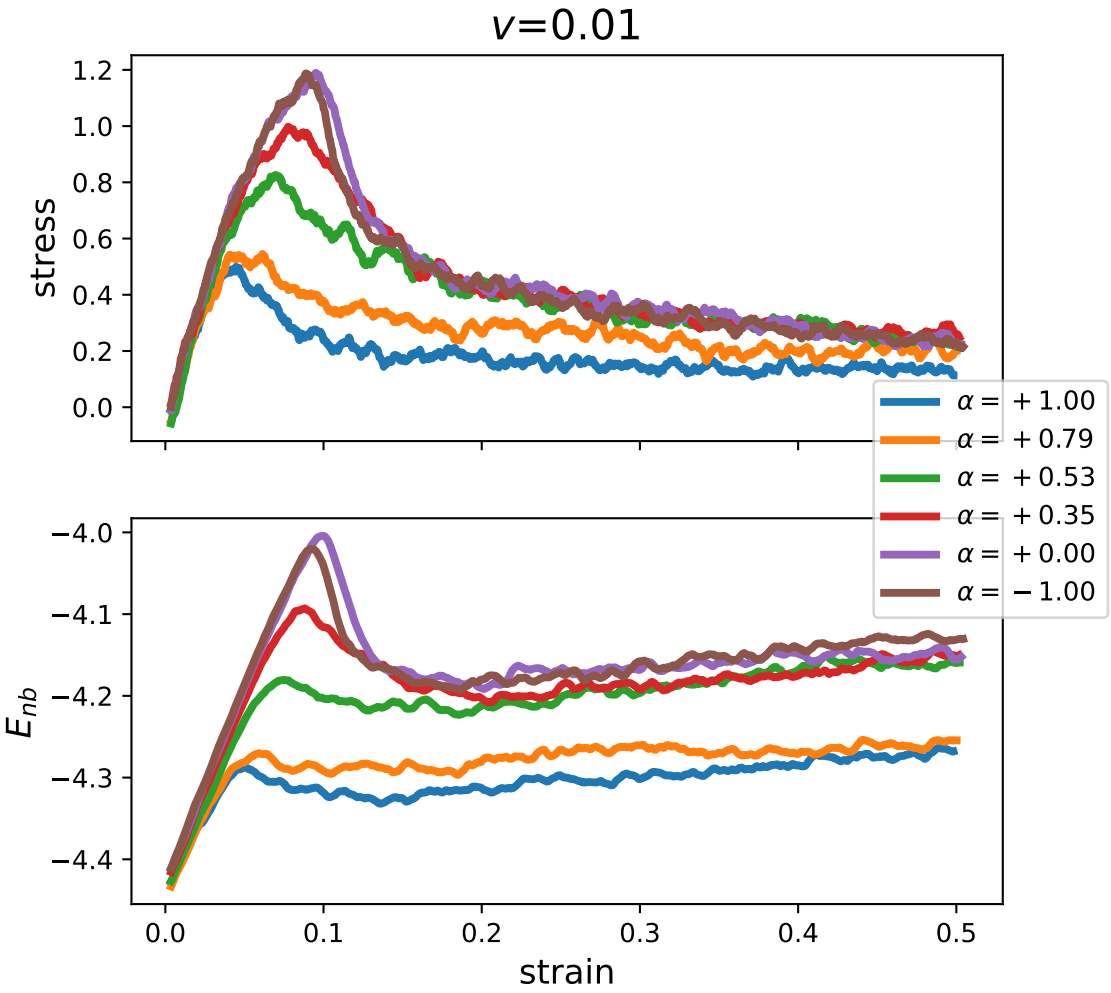


Figure 1: Plots of the initial stress-strain curves and non-bonding energy per atom for all systems, for slow pulling velocity ($v = 0.01$).

As the surface morphologies change towards increasingly segregated configurations of the $S$ and $W$ sites ($\alpha > 0$), we see a progressive degradation in the mechanical properties of the sandwiched films. The most segregated surfaces display a roughly 50% decrease in both the yield stress and the yield strain. The toughness of the adhesive layers, as measured by the mechanical work to separate the surfaces (integral of the stress-strain curves) is also reduced accordingly. After the yield point, the stress decreases and approaches a plateau value, which depends again on the surface morphology. The plateau is in fact a gently decreasing slope, which continues until extremely large deformations. The full breakup of the adhesive films

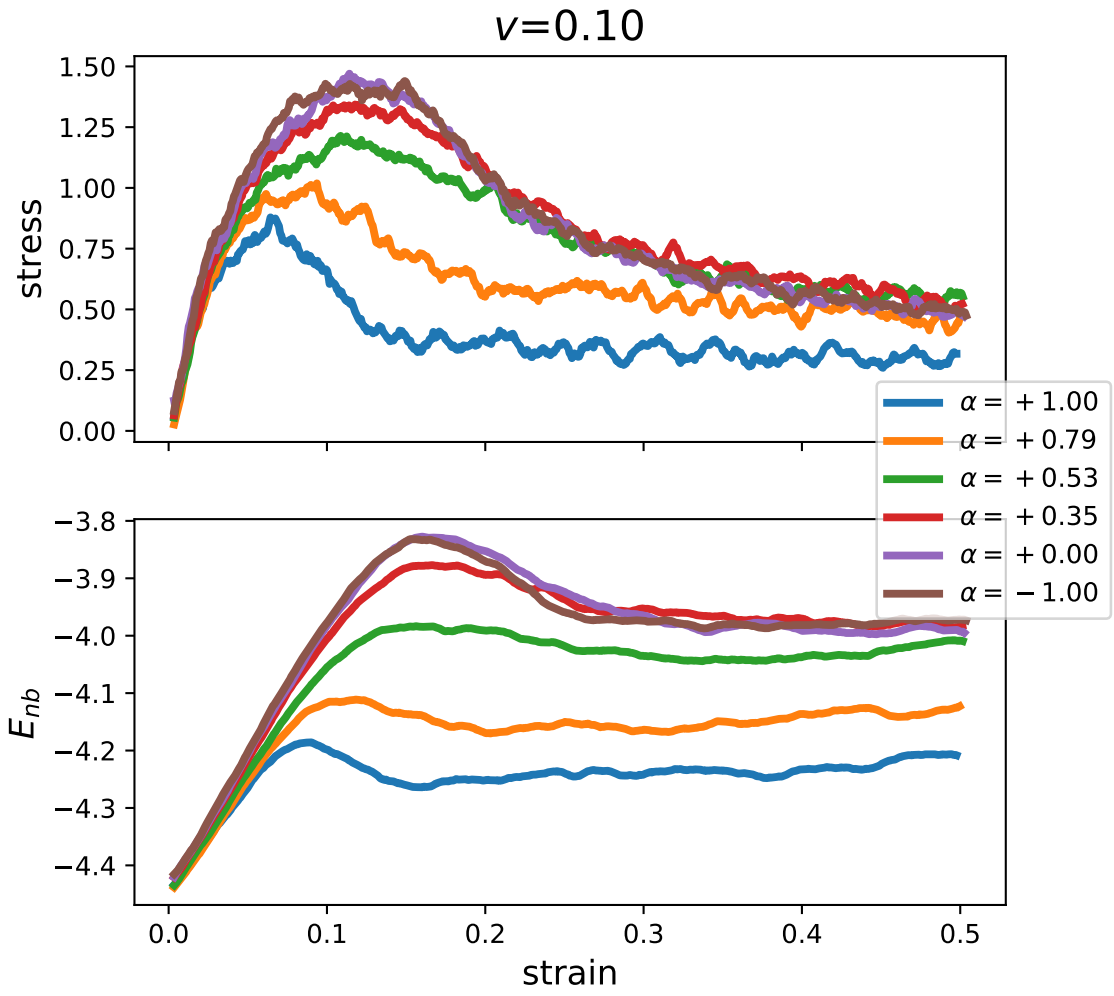


Figure 2: Plots of the initial stress-strain curves and non-bonding energy per atom for all systems, for fast pulling velocity ($v = 0.10$).

occurs only for $\epsilon \simeq 14$ (see again SI.4 and SI.4). In terms of surface-surface separation this correspond to $z \simeq 180$, well above the fully extended length of the individual chains.

Figure 3 illustrates the typical behavior, for a system with an intermediate degree of segregation ($\alpha = 0.53$). The snapshots clearly show the detachment of the polymer from the weak spots on the surfaces, corresponding to patches with a high concentration of $W$ sites. The detachment could also be described as the nucleation of voids within the interfacial polymer layers. The voids form already at small deformations, corresponding to the yield points in the stress-strain curves. The interfacial voids gradually evolve into large cavities. Similar but much larger voids have also been observed by optical microscopy on PSA's.[15–17] Eventually, the polymer forms fibrils bridging the surfaces, which progressively become thinner as they stretch. This long fibrillation phase corresponds to the broad plateau in the stress. In the late stages of deformation, the fibrils contains just a few chains, none of which is long enough to span their entire length. In the end each fibril breaks somewhere in the middle and the remaining polymer chains are quickly reeled back in by the surfaces, forming two thin adsorbed layers.

The initial nuclei are not easily observed using a conventional representation, but they can be highlighted by resorting to a Voronoi analysis.[61] The "voids" can be associated with the beads whose Voronoi volume is larger than a threshold value, that here we set equal to 2.00. Figure 4 shows the results of such an analysis, for the two extreme cases ($\alpha = \pm 1$). The voids tend to form on $W$-rich patches, provided they are large enough. Increasing the degree of segregation between the $W$ and $S$ sites lowers the barrier to void nucleation. As a result, the yield stress and the yield strain decrease. On the same surfaces, however, there are equally large patches with a stronger polymer-surface interaction. The polymer adsorbed on these patches is not susceptible to yield. The net result is that rupture of the polymer films between the segregated surfaces can be described as a mixtures of adhesive and cohesive failure, corresponding to the loss of polymer-surface and polymer-polymer interactions. Instead, when there is a fine interdispersion of $W$ and $S$ sites ($\alpha \leq 0$),

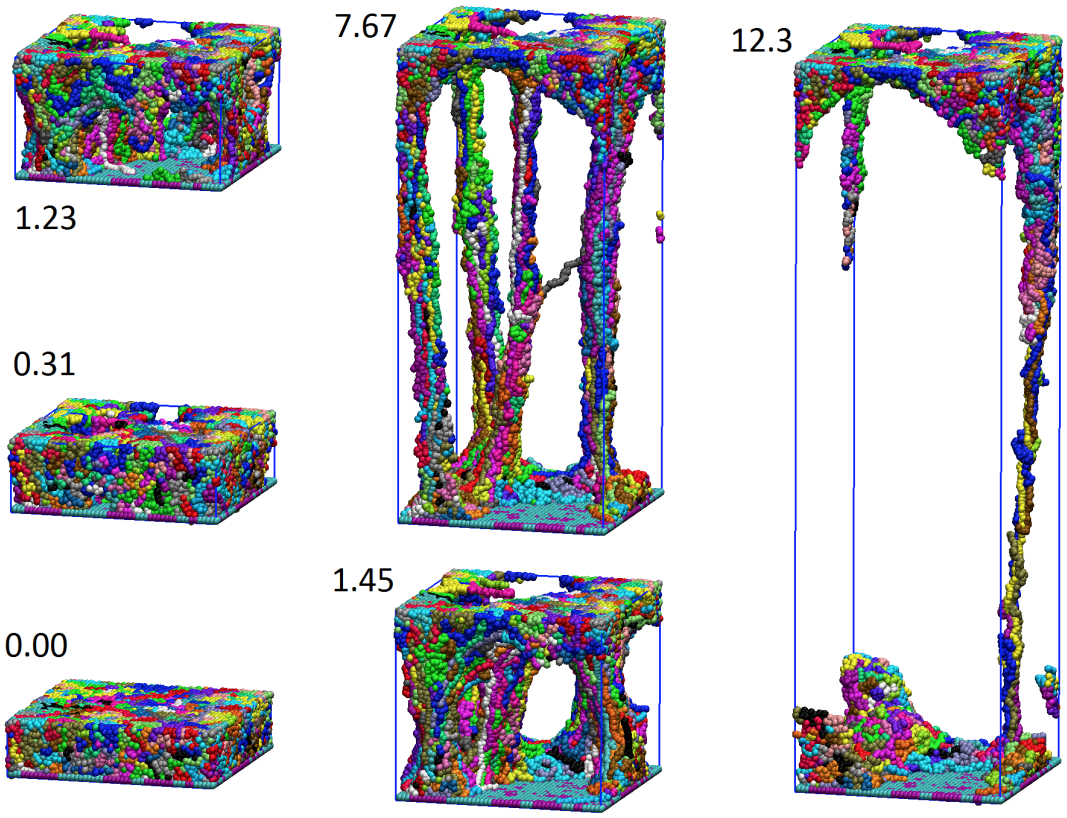


Figure 3: Evolution of polymer film between surfaces with $\alpha = 0.53$, as they are pulled apart at $v = 0.1$. The strain values ($\epsilon$) are reported next to each snapshot. The upper surface has been deleted for clarity.

the polymer-substrate interactions are always strong enough to prevent adhesive failure. The voids are preferentially nucleated within the polymer, and the failure mechanism is entirely of the cohesive type. Indeed, the maximum stresses that are recorded in these cases are very close to those observed in control simulations on the bulk polymer, at the same deformation rates (see Figure SI.5).

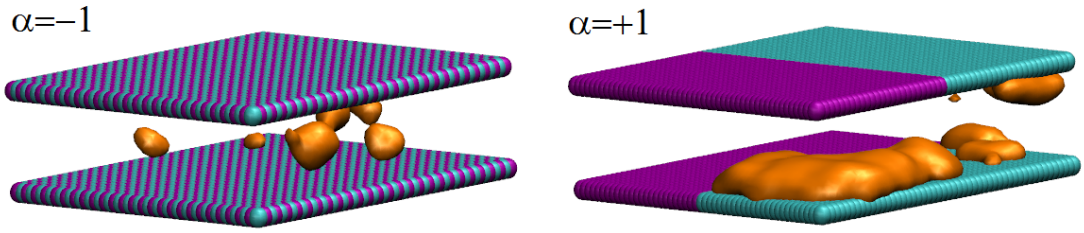


Figure 4: Visualization of the cavitation nuclei at $\epsilon = 0.12$, for two different surfaces.

Our interpretation of the failure mechanisms of the films is supported by further analysis of the non-bonded interactions. Figure 5 illustrates the strain-dependence of their individual polymer-polymer and polymer-surface components. The films with the highest adhesion strengths show a modest change in the polymer-surface interactions, alongside a large variation in the polymer-polymer ones. Thus, in these cases the initial cavities are largely formed within the polymer, in the middle of the films. There is actually a small "hump" in the polymer-surface interactions when $\alpha = -1.00$, at a strain which corresponds to the maximum in the polymer-polymer curve. Thus, in this case there appears to be a limited, temporary separation between the polymer and the surfaces. Interestingly, this hump is almost absent in the random surface ($\alpha = 0.00$), indicating that its interface with the polymer is even superior in terms of mechanical stability. The system with moderate segregation of the $W$ and $S$ sites ($\alpha = +0.35$) is still quite good, from this point of view. A clear degradation in the stability of the adhesive interface occurs on increasing the segregation even further ($\alpha = +0.53$ and 0.79). Notice that the polymer-surface interactions are no longer recovered, past the yield point. In the fully segregated system ($\alpha = +1.00$), the surfaces can be separated with a relatively modest variation in the polymer-polymer interactions, while

the changes in the polymer-surface interactions increase and become almost comparable to them.

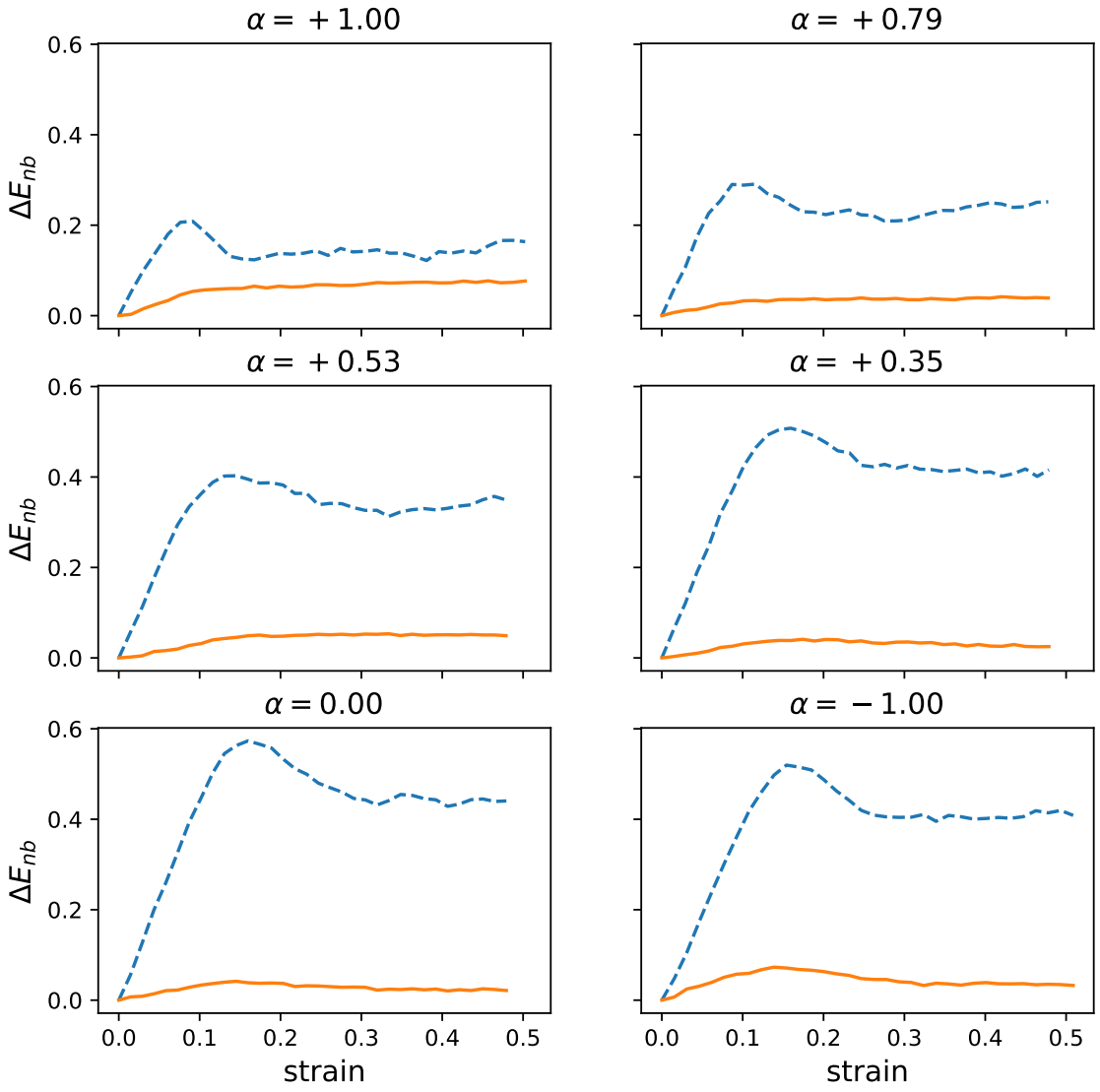


Figure 5: Variation in the polymer-polymer (dashed) and polymer-surface (continuous) non-bonded interaction, from the simulations with fast separation ($v = 0.10$). The non-bonded energies are normalized by the total number of atoms.

As a final step in the analysis of the results, we present histograms of the individual chains' contributions to the overall stress. See Figure 6 for three representative cases, for both fast and slow deformation speeds. These graphs have been obtained at $\epsilon = 0.11$, in the neighbourhood of the yield points. The histograms are fairly symmetric, Gaussian-

like distributions. The Gaussian shape is expected from the central limit theorem, as the stress on a chain is the sum of many, largely uncorrelated contributions from its constituent beads.[62] Here we have adopted a logarithmic scale for the vertical axes, to highlight the tails in the distributions, representing a small fraction of highly stressed chains. The center of the distributions always occur at positive values, as expected. However, there are also many chains making a negative contribution to the stress. This means that they are actually pushing the surfaces apart, rather than pulling them together. This is understandable, considering the effect of confinement on their conformational entropy. The fraction of these chains increases with $\alpha$, presumably due to chains which are adsorbed on the weakly binding patches. For a given surface, it also grows on decreasing the rate of deformation, giving the chains more time to relax towards equilibrium. The net effect is the systematic variation of the yield stress, which was previously discussed.

**Conclusions.** Our MD simulations on a simple model system provide a clear demonstration of the effect of surface morphology on the adhesive properties of polymer films. Significant and systematic differences are observed among surfaces sharing the same "chemistry", represented here by the fractions of weakly and strongly interacting sites, but with different spatial arrangements. A small change in surface morphology can have a major effect on the barrier for interfacial nucleation of nanoscale voids, leading from a cohesive to a mixed adhesive-cohesive failure of the films. The adhesive properties of a completely random surface are very similar or even superior to those of a perfectly ordered one, as in both cases the scale of the heteogeneities is too small and the surface effectively behaves as if it were homogeneous. The effect of the heterogeneity emerges on going to more patchy, nanosegregated surfaces, and interestingly it tends to weaken the mechanical properties of the adhesive film. We stress that, on the basis of macroscale observations of the final state of the system, the failure would still appear to be of the cohesive type, since the polymer is eventually distributed over both surfaces. Thus, our simulations provide an interesting example of model adhesive films whose "cohesive" behavior crucially depends on the polymer-surface

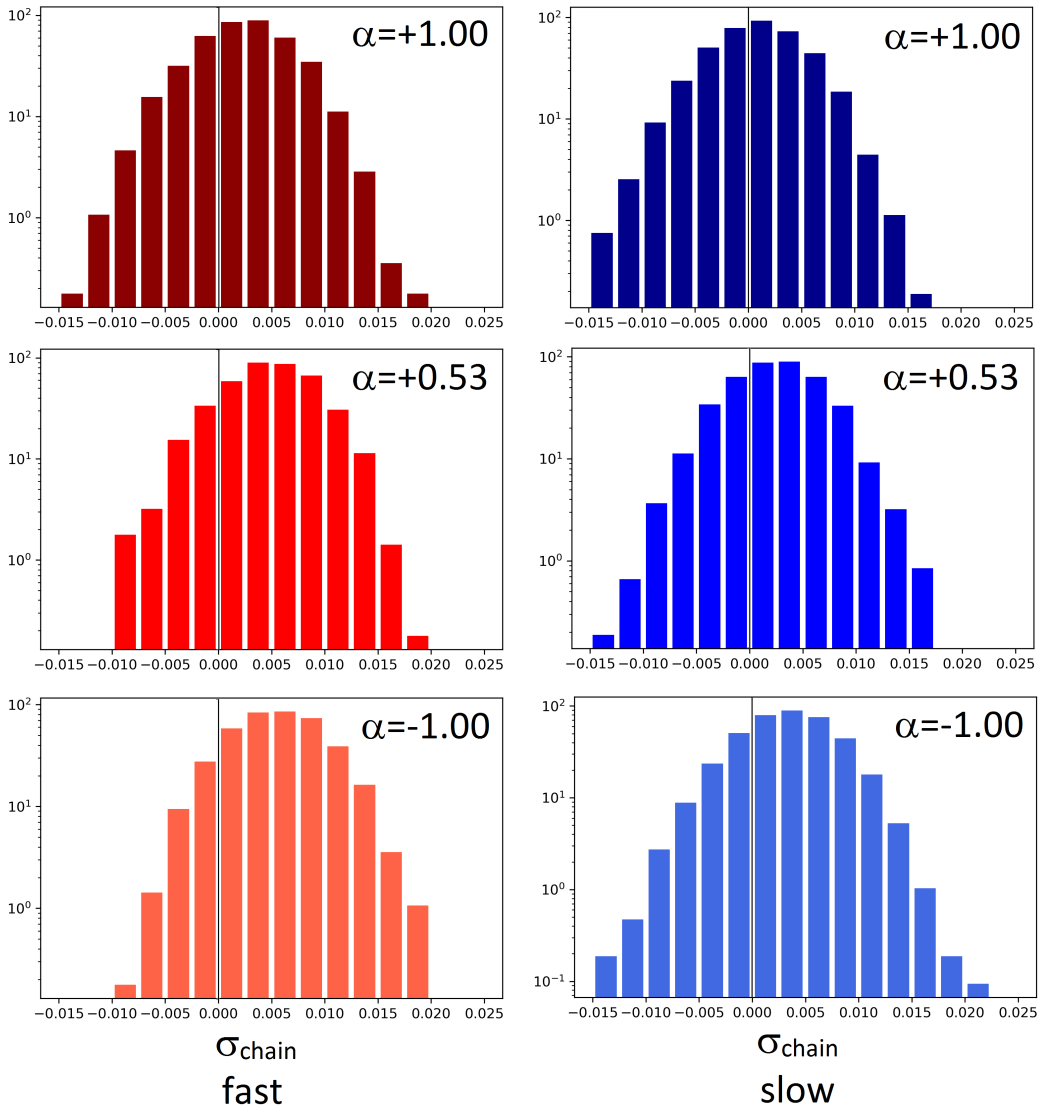


Figure 6: Histograms of the stress borne by individual polymer chains in three representative systems (see the $\alpha$ values), for fast and slow deformations (left and right, respectively). The thin vertical lines mark the zero stress.

interactions, as well as the nanoscale morphology of the adherend. We are not aware of any real adhesive films that is already known behave in this way. Demonstrating it might be experimentally difficult, as it involves the capability to finely tune the morphology of the surfaces and, at the same time, to observe their debonding mechanisms at the nanoscale, in situ and in real time. One possibility might be in the observation of nucleation and growth of voids in polymer nanocomposites, by real-time small-angle X-ray scattering.[37]

Our simulations raise interesting questions in the fields of adhesion science, tribology and rubber reinforcement by nanoparticles. For example, it would be interesting to observe the role of surface heterogeneities also under shear and cyclic deformations. We intend to pursue them through more extensive simulations, adding variables such as molecular weight and chain scission to the problem. It would also be interesting to investigate the effect of heterogeneity in the chemical composition and morphology of the polymer films, through the inclusion of monomers capable of interacting with a solid surface by hydrogen bonding and coordinative bonds.[63] Such models might be relevant also for protein-based adhesion of marine organisms. In the meantime, we hope that the present results will stimulate further experimental efforts on polymer adhesion to surfaces with controlled nanoscale morphologies.

## Acknowledgement

GR thanks Bruno Zappone (CNR-Nanotec Cosenza) for stimulating discussions.

## Supporting Information Available

Conversion from Lennard-Jones to conventional S.I. units, additional plots and figures. This information is available free of charge on `https://pubs.acs.org`.

# References


(1) Pocius, A. V. *Adhesion and Adhesives Technology, 3rd edition*; Hanser Verlag, Munich, 2012.

(2) Shull, K. R. Contact mechanics and the adhesion of soft solids. *Materials Science and Engineering: R: Reports* **2002**, *36*, 1–45.

(3) Ghatak, A.; Vorvolakos, K.; She, H.; Malotky, D. L.; Chaudhury, M. K. Interfacial Rate Processes in Adhesion and Friction. *The Journal of Physical Chemistry B* **2000**, *104*, 4018–4030.

(4) Israelachvili, J. N. *Intermolecular and surface forces, 3rd edition*; Academic Press, 2011.

(5) Luengo, G.; Schmitt, F.-j.; Hill, R.; Israelachvili, J. Thin Film Rheology and Tribology of Confined Polymer Melts: Contrasts with Bulk Properties. *Macromolecules* **1997**, *30*, 2482–2494.

(6) Benz, M.; Rosenberg, K. J.; Kramer, E. J.; Israelachvili, J. N. The Deformation and Adhesion of Randomly Rough and Patterned Surfaces. *The Journal of Physical Chemistry B* **2006**, *110*, 11884–11893.

(7) Wang, X. P.; Xiao, X.; Tsui, O. K. C. Surface Viscoelasticity Studies of Ultrathin Polymer Films Using Atomic Force Microscopic Adhesion Measurements. *Macromolecules* **2001**, *34*, 4180–4185.

(8) Lee, B. P.; Messersmith, P.; Israelachvili, J.; Waite, J. Mussel-Inspired Adhesives and Coatings. *Annual Review of Materials Research* **2011**, *41*, 99–132.

(9) Bilotto, P.; Labate, C.; De Santo, M. P.; Deepankumar, K.; Miserez, A.; Zappone, B. Adhesive Properties of Adsorbed Layers of Two Recombinant Mussel Foot Proteins with Different Levels of DOPA and Tyrosine. *Langmuir* **2019**, *35*, 15481–15490.

(10) Guo, Q.; Chen, J.; Wang, J.; Zeng, H.; Yu, J. Recent progress in synthesis and application of mussel-inspired adhesives. *Nanoscale* **2020**, *12*, 1307–1324.

(11) North, M. A.; Del Grosso, C. A.; Wilker, J. J. High Strength Underwater Bonding with Polymer Mimics of Mussel Adhesive Proteins. *ACS Applied Materials and Interfaces* **2017**, *9*, 7866–7872.

(12) Zosel, A. Adhesion and tack of polymers: Influence of mechanical properties and surface tensions. *Colloid & Polymer Science* **1985**, *263*, 541–553.

(13) Shull, K. R.; Creton, C. Deformation behavior of thin, compliant layers under tensile loading conditions. *Journal of Polymer Science Part B: Polymer Physics* **2004**, *42*, 4023–4043.

(14) Gay, C.; Leibler, L. On Stickiness. *Physics Today* **1999**, *52*, 48–52.

(15) Lakrout, H.; Sergot, P.; Creton, C. Direct observation of cavitation and fibrillation in a probe tack experiment on model acrylic pressure-sensitive-adhesives. *Journal of Adhesion* **1999**, *69*, 307–359.

(16) Yamaguchi, T.; Koike, K.; Doi, M. In situ observation of stereoscopic shapes of cavities in soft adhesives. *Europhysics Letters (EPL)* **2007**, *77*, 64002.

(17) Nase, J.; Creton, C.; Ramos, O.; Sonnenberg, L.; Yamaguchi, T.; Lindner, A. Measurement of the receding contact angle at the interface between a viscoelastic material and a rigid surface. *Soft Matter* **2010**, *6*, 2685.

(18) Persson, B. N. J.; Albohr, O.; Heinrich, G.; Ueba, H. Crack propagation in rubber-like materials. *Journal of Physics: Condensed Matter* **2005**, *17*, R1071–R1142.

(19) Yamaguchi, T.; Morita, H.; Doi, M. Modeling on debonding dynamics of pressure-sensitive adhesives. *The European physical journal. E, Soft matter* **2006**, *20*, 7–17.

(20) Yamaguchi, T.; Creton, C.; Doi, M. Simple model on debonding of soft adhesives. *Soft Matter* **2018**, *14*, 6206–6213.

(21) Huang, H.; Dasgupta, A.; Singh, N. Predictive mechanistic model for single-layered pressure-sensitive adhesive (PSA) joints. *The European Physical Journal E* **2020**, *43*, 59.

(22) Gersappe, D.; Robbins, M. O. Where do polymer adhesives fail? *Europhysics Letters* **1999**, *48*, 150–155.

(23) Baljon, A. R. C.; Vorselaars, J.; Depuy, T. J. Computational Studies of Contact Time Dependence of Adhesive Energy Due to Redistribution of the Locations of Strong Specific Interfacial Interactions. *Macromolecules* **2004**, *37*, 5800–5806.

(24) Froltsov, V. A.; Klüppel, M.; Raos, G. Molecular dynamics simulation of rupture in glassy polymer bridges within filler aggregates. *Physical Review E* **2012**, *86*, 041801/1–10.

(25) Solar, M.; Qin, Z.; Buehler, M. J. Molecular mechanics and performance of crosslinked amorphous polymer adhesives. *Journal of Materials Research* **2014**, *29*, 1077–1085.

(26) Jin, K.; López Barreiro, D.; Martin-Martinez, F. J.; Qin, Z.; Hamm, M.; Paul, C. W.; Buehler, M. J. Improving the performance of pressure sensitive adhesives by tuning the crosslinking density and locations. *Polymer* **2018**, *154*, 164–171.

(27) Bansal, A.; Yang, H.; Li, C.; Cho, K.; Benicewicz, B. C.; Kumar, S. K.; Schadler, L. S. Quantitative equivalence between polymer nanocomposites and thin polymer films. *Nature Materials* **2005**, *4*, 693–698.

(28) Rittigstein, P.; Priestley, R. D.; Broadbelt, L. J.; Torkelson, J. M. Model polymer nanocomposites provide an understanding of confinement effects in real nanocomposites. *Nature Materials* **2007**, *6*, 278–282.

(29) Allegra, G.; Raos, G.; Vacatello, M. Theories and simulations of polymer-based nanocomposites: From chain statistics to reinforcement. *Progress in Polymer Science* **2008**, *33*, 683–731.

(30) Jancar, J.; Douglas, J.; Starr, F. W.; Kumar, S.; Cassagnau, P.; Lesser, A.; Sternstein, S. S.; Buehler, M. Current issues in research on structure–property relationships in polymer nanocomposites. *Polymer* **2010**, *51*, 3321–3343.

(31) Vilgis, T. A.; Heinrich, G.; Klüppel, M. *Reinforcement of polymer nano-composites: theory, experiments and applications*; Cambridge University Press, 2009.

(32) Donnet, J.-B.; Bandal, R. C.; Wang, M.-J. *Carbon black: science and technology, 2nd edition*; Marcel Dekker, 1993.

(33) Schröder, A.; Klüppel, M.; Schuster, R. H. Characterisation of surface activity of carbon black and its relation to polymer-filler interaction. *Macromolecular Materials and Engineering* **2007**, *292*, 885–916.

(34) Koga, T.; Hashimoto, T.; Takenaka, M.; Aizawa, K.; Amino, N.; Nakamura, M.; Yamaguchi, D.; Koizumi, S. New Insight into Hierarchical Structures of Carbon Black Dispersed in Polymer Matrices: A Combined Small-Angle Scattering Study. *Macromolecules* **2008**, *41*, 453–464.

(35) Litvinov, V. M.; Orza, R. A.; Kluppel, M.; van Duin, M.; Magusin, P. C. M. M. Rubber–Filler Interactions and Network Structure in Relation to Stress–Strain Behavior of Vulcanized, Carbon Black Filled EPDM. *Macromolecules* **2011**, *44*, 4887–4900.

(36) Vilgis, T. A. Time scales in the reinforcement of elastomers. *Polymer* **2005**, *46*, 4223–4229.

(37) Zhang, H.; Scholz, A. K.; de Crevoisier, J.; Vion-Loisel, F.; Besnard, G.; Hexemer, A.; Brown, H. R.; Kramer, E. J.; Creton, C. Nanocavitation in Carbon Black Filled

Styrene–Butadiene Rubber under Tension Detected by Real Time Small Angle X-ray Scattering. *Macromolecules* **2012**, *45*, 1529–1543.

(38) Hagita, K.; Morita, H.; Takano, H. Molecular dynamics simulation study of a fracture of filler-filled polymer nanocomposites. *Polymer* **2016**, *99*, 368–375.

(39) Baumgärtner, A.; Muthukumar, M. Effects of surface roughness on adsorbed polymers. *The Journal of Chemical Physics* **1991**, *94*, 4062.

(40) Baumgaertner, A.; Muthukumar, M. Polymers in Random Media. *Advances in chemical physics* **1996**, *94*, 625–708.

(41) Alcoutlabi, M.; McKenna, G. B. Effects of confinement on material behaviour at the nanometre size scale. *Journal of Physics: Condensed Matter* **2005**, *17*, R461.

(42) Baschnagel, J.; Varnik, F. Computer simulations of supercooled polymer melts in the bulk and in confined geometry. *Journal of Physics: Condensed Matter* **2005**, *17*, R851.

(43) Torres, J.; Nealey, P.; De Pablo, J. Molecular simulation of ultrathin polymeric films near the glass transition. *Physical Review Letters* **2000**, *85*, 3221.

(44) Hanakata, P. Z.; Douglas, J. F.; Starr, F. W. Interfacial mobility scale determines the scale of collective motion and relaxation rate in polymer films. *Nature communications* **2014**, *5*, 4163.

(45) Raos, G.; Sluckin, T. J. Pulling Polymers on Energetically Disordered Surfaces: Molecular Dynamics Tests of Linear and Non-linear Response. *Macromolecular Theory and Simulations* **2013**, *22*, 225–237.

(46) Raos, G.; Idé, J. Impact of interaction strength and surface heterogeneity on the dynamics of adsorbed polymers. *ACS Macro Letters* **2014**, *3*, 721–726.

(47) Pastore, R.; Raos, G. Glassy dynamics of a polymer monolayer on a heterogeneous disordered substrate. *Soft matter* **2015**, *11*, 8083–8091.

(48) Pastore, R.; David, A.; Casalegno, M.; Greco, F.; Raos, G. Influence of wall heterogeneity on nanoscopically confined polymers. *Physical Chemistry Chemical Physics* **2019**, *21*, 772–779.

(49) Huang, K. *Statistical Mechanics, 2nd edition*; John Wiley & Sons, New York, 1987.

(50) Allen, M. P.; Tildesley, D. J. *Computer simulation of liquids, 2nd edition*; Oxford University Press, 2017.

(51) Warren, B. E. *X-ray Diffraction*; Dover Publications, 1990.

(52) Cowley, J. An approximate theory of order in alloys. *Physical Review* **1950**, *77*, 669.

(53) Kremer, K.; Grest, G. S. Dynamics of entangled linear polymer melts: A molecular-dynamics simulation. *The Journal of Chemical Physics* **1990**, *92*, 5057–5086.

(54) Mackura, M. E.; Simmons, D. S. Enhancing heterogenous crystallization resistance in a bead-spring polymer model by modifying bond length. *Journal of Polymer Science Part B: Polymer Physics* **2014**, *52*, 134–140.

(55) Huang, Q.; Hassager, O. Polymer liquids fracture like solids. *Soft Matter* **2017**, *13*, 3470–3474.

(56) Shinoda, W.; Shiga, M.; Mikami, M. Rapid estimation of elastic constants by molecular dynamics simulation under constant stress. *Physical Review B - Condensed Matter and Materials Physics* **2004**, *69*, 16–18.

(57) Plimpton, S. Fast parallel algorithms for short-range molecular dynamics. *Journal of computational physics* **1995**, *117*, 1–19.

(58) Humphrey, W.; Dalke, A.; Schulten, K. VMD – Visual Molecular Dynamics. *Journal of Molecular Graphics* **1996**, *14*, 33–38.

(59) Thompson, A. P.; Plimpton, S. J.; Mattson, W. General formulation of pressure and stress tensor for arbitrary many-body interaction potentials under periodic boundary conditions. *Journal of Chemical Physics* **2009**, *131*, 1–6.

(60) Landau, L. D.; Lifshitz, E. M. *Statistical physics, part 1*, third edition ed.; Elsevier,, 1980.

(61) Rycroft, C. H. VORO++: A three-dimensional Voronoi cell library in C++. *Chaos* **2009**, *19*, 2008–2009.

(62) Reif, F. *Fundamentals of Statistical and Thermal Physics*; McGraw-Hill, 1965.

(63) Dunbar, M.; Keten, S. Energy Renormalization for Coarse-Graining a Biomimetic Copolymer, Poly(catechol-styrene). *Macromolecules* **2020**, *53*, 9397–9405.

# Graphical TOC Entry

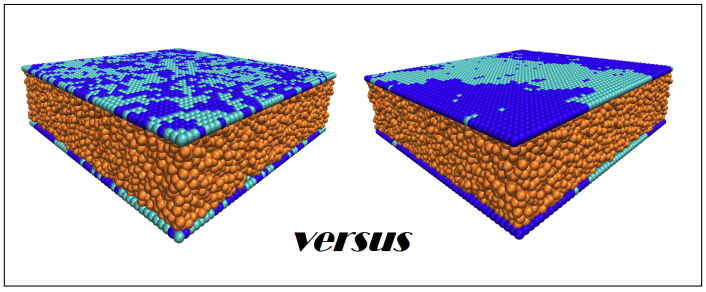


Which is the optimal surface morphology for polymer-mediated adhesion?

Supplementary information for:

# Polymer-mediated adhesion: nanoscale surface morphology and failure mechanisms

*Alberto Baggioli, Mosè Casalegno, Alessio David, Marta Pasquini and Guido Raos*
Politecnico di Milano, Milano, Italy

**Conversion from Lennard-Jones to conventional SI units.**

The mapping from LJ to SI units requires a decision about the values attached to specific quantities, such as the bead diameter $\sigma$. The Kremer-Grest bead-and-spring model [1] is highly simplified. It was developed with computational simplicity in mind, without attempting to reproduce the properties of any specific polymer. The simplification is possible thanks to the universal behavior of polymers, at large length and long time scales. Its adaptation to specific polymers is possible, but it requires at least the introduction of some stiffness, through a bond bending energy.[2]

In view of the previous considerations, any mapping of the Kremer-Grest model will always be somewhat approximate. Nonetheless, adopting Kröger's suggested mapping for polystyrene,[3] we have the following conversion factors:

- Distance: $\sigma$ = 0.97 nm
- Mass: $m$ = 364 g/mol
- Energy: $\varepsilon_{PP}/k_B$ = 490 K, or equivalently $\varepsilon_{PP}$= 4.07 kJ/mol.
- Density: $m/\sigma^3$ = 6.6 g/cm$^3$ = 6.6 Mg/m$^3$.
- Stress: $\varepsilon_{PP}/\sigma^3$ = 7.4 MPa
- Time: $\tau = \sqrt{m\sigma^2/\varepsilon_{PP}}$ = 9.1 ps
- Velocity: $\sigma/\tau$ = 107 m/s
- Strain rate: $1/\tau$ = 0.11 ps$^{-1}$.

This mapping is approximate, also because in the present simulations we have adopted a slightly shorter FENE bond length [4] and we have included the attractive tail of the LJ interaction, which is absent in the conventional Kremer-Grest model. Nonetheless, the mapped parameters appear to be reasonable. The molecular mass of the polymer chains is 47 kDa. The initial inter-surface distance would be equal to 12.6 nm. The "fast" and "slow" pulling speeds are equal to 10.7 and 1.17 m/s, respectively. The stresses recorded in the simulations are in the 1-10 MPa range.

[1] Kremer, K.; Grest, G. S. Dynamics of Entangled Linear Polymer Melts: A Molecular-dynamics Simulation. *J. Chem. Phys.* **1990**, *92* (8), 5057–5086. https://doi.org/10.1063/1.458541
[2] Everaers, R.; Karimi-Varzaneh, H. A.; Fleck, F.; Hojdis, N.; Svaneborg, C. Kremer–Grest Models for Commodity Polymer Melts: Linking Theory, Experiment, and Simulation at the Kuhn Scale. *Macromolecules* **2020**, *53* (6), 1901–1916. https://doi.org/10.1021/acs.macromol.9b02428
[3] Kröger, M. Simple Models for Complex Nonequilibrium Fluids. *Phys. Rep.* **2004**, *390* (6), 453–551. https://doi.org/10.1016/j.physrep.2003.10.014
[4] MacKura, M. E.; Simmons, D. S. Enhancing Heterogenous Crystallization Resistance in a Bead-Spring Polymer Model by Modifying Bond Length. *J. Polym. Sci. Part B Polym. Phys.* **2014**, *52* (2), 134–140. https://doi.org/10.1002/polb.23398

**Additional plots and figures**

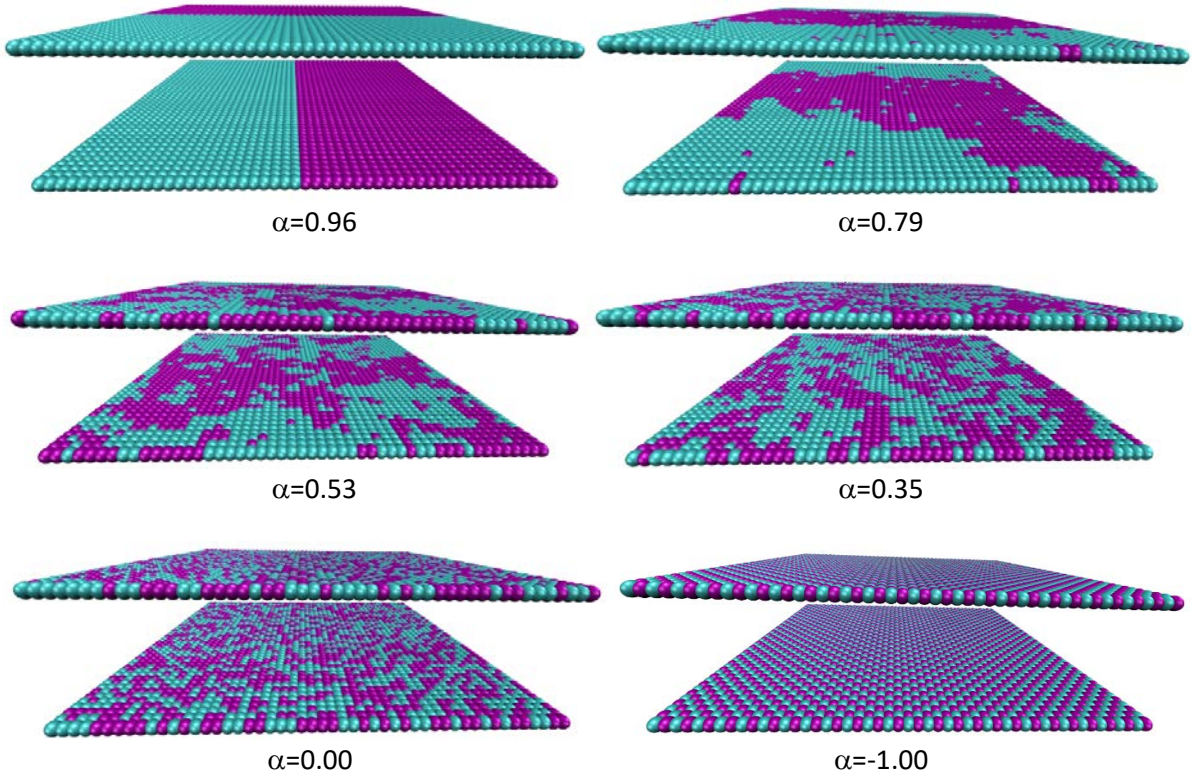


Figure SI.1: morphologies of the simulated surfaces.

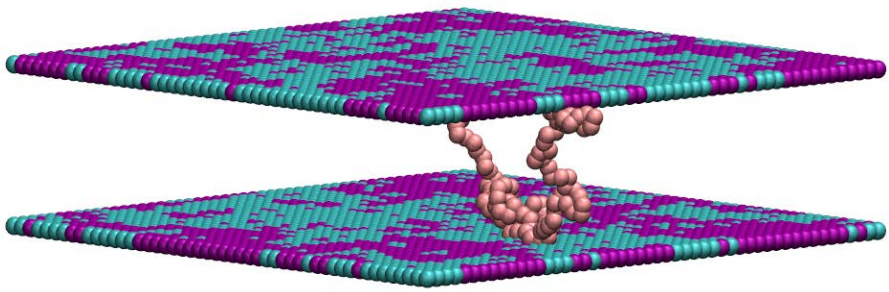

Figure SI.2: one bridging chain between two surfaces.

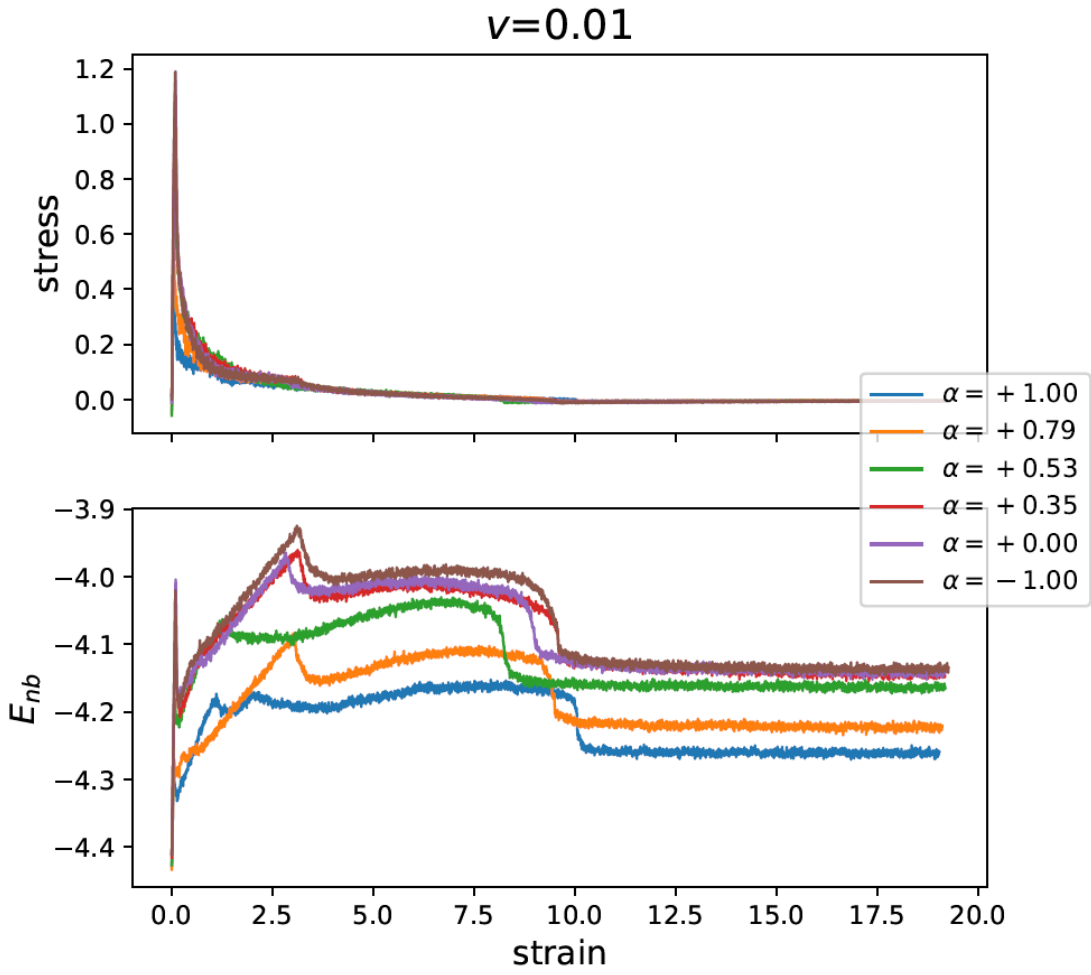


Figure SI.3: Full stress-strain curves and non-bonding energy plots for all systems, for "slow" pulling velocity (v=0.01, corresponding to $\dot{\varepsilon}=7.7\times10^{-4}$).

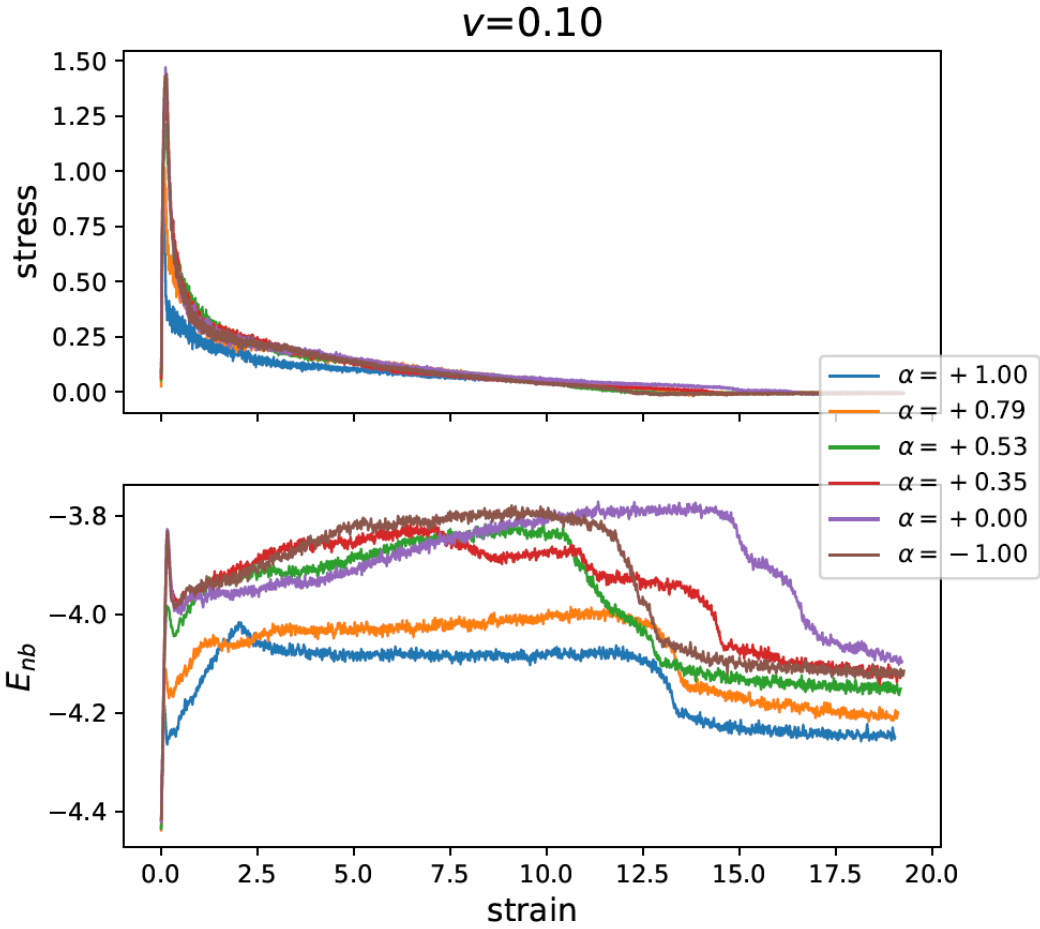


Figure SI.4: Full stress-strain curves and non-bonding energy plots for all systems, for "fast" pulling velocity (v=0.10, corresponding to $\dot{\varepsilon}$=7.7×10$^{-3}$).

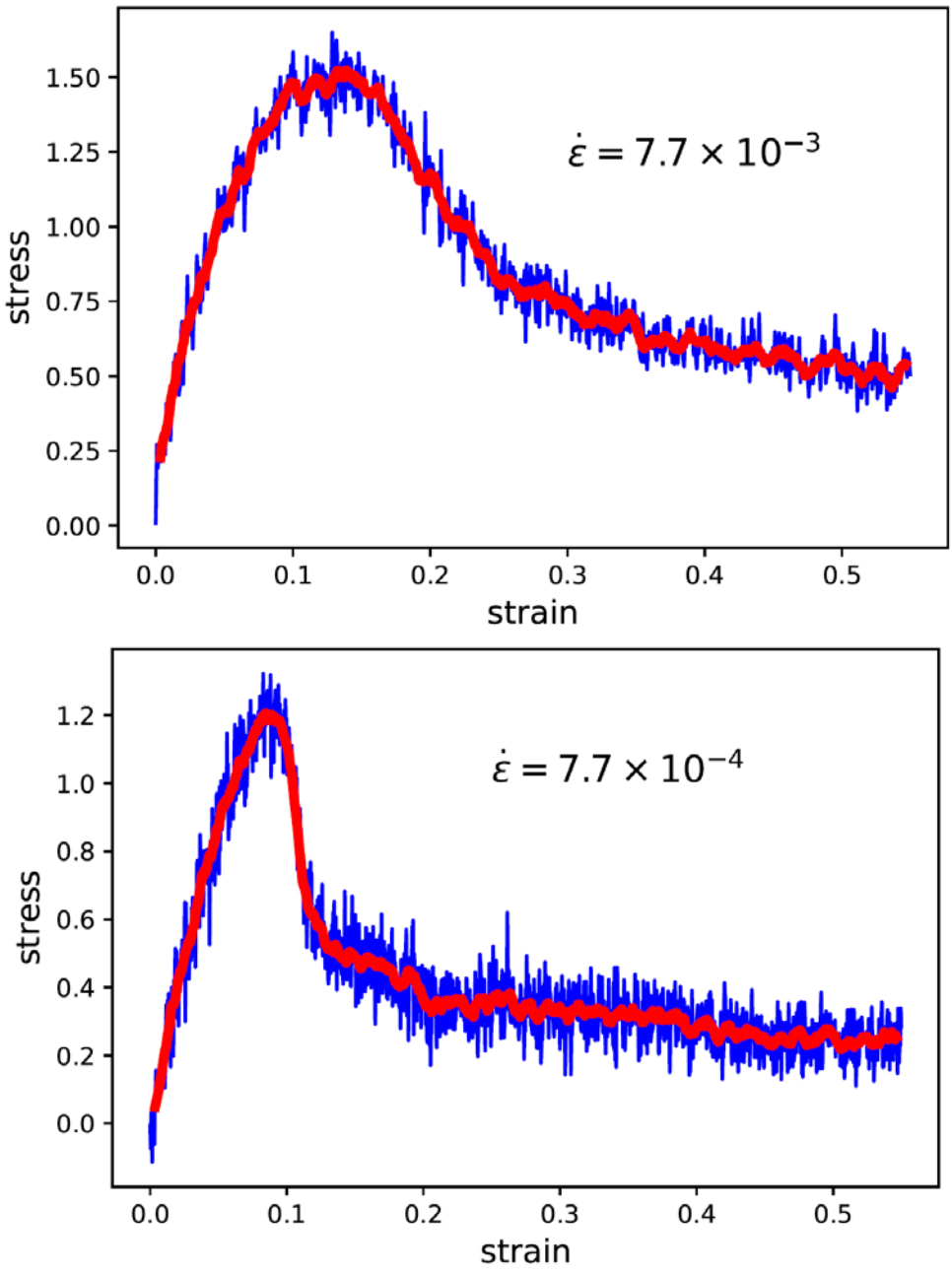


Figure SI.5: Initial stress-strain curves for the bulk polymer, for fast and slow deformations (above and below, respectively). The blue lines represent the instantaneous values, the red lines the batch or running averages over 100 timesteps (for $\dot{\varepsilon}$=7.7×10$^{-3}$, corresponding to v=0.10) or 1000 timesteps (for $\dot{\varepsilon}$=7.7×10$^{-4}$, corresponding to v=0.01). The system contains 250 chains, with full three-dimensional boundary conditions. Before carrying out the deformation, it was equilibrated at T=1.0 and P=0.0. In analogy with the simulations of the confined polymer, the system is stretched at the indicated rates along one direction (e.g., *z*), while leaving the periodicity along the orthogonal directions unchanged (i.e., imposing a Poisson ratio σ=0.0).